# Localized Epitaxial Growth of 402 V Breakdown Voltage Quasi-Vertical GaN-on-Si p-n Diode on 200 mm-Diameter Wafers

Thomas Kaltsounis, Mohammed El Amrani, David Plaza Arguello, Hala El Rammouz, Vishwajeet Maurya, Matthieu Lafossas, Simona Torrengo, Helge Haas, Laurent Mendizabal, Alain Gueugnot, et al.

physica status solidi a
www.pss-a.com

# Localized Epitaxial Growth of 402 V Breakdown Voltage Quasi-Vertical GaN-on-Si p-n Diode on 200 mm-Diameter Wafers

*Thomas Kaltsounis,* Mohammed El Amrani, David Plaza Arguello, Hala El Rammouz, Vishwajeet Maurya, Matthieu Lafossas, Simona Torrengo, Helge Haas, Laurent Mendizabal, Alain Gueugnot, Denis Mariolle, Thomas Jalabert, Julien Buckley, Yvon Cordier, and Matthew Charles*

**Localized epitaxy of gallium nitride (GaN) on silicon (Si) wafers is an efficient way to relax elastically the tensile stress generated in the GaN layer after growth, allowing epitaxy of thick layers for the fabrication of vertical power devices operating at high voltage. In this study, a 4.7 µm-thick GaN layer is grown by metal–organic vapor phase epitaxy on 200 mm-diameter Si wafers for the fabrication of quasi-vertical Schottky and p-n diodes. The uniformity of the doping concentration in the layer is mapped spatially by scanning spreading resistance microscopy, while scanning capacitance microscopy illustrates the differently doped regions in the p-n diode. The net doping concentration is extracted by capacitance–voltage (*C–V*) measurements and it is found to be about $3 \times 10^{16}$ cm$^{-3}$. On a 140 µm-diameter quasi-vertical p-n diode, destructive breakdown occurs at 402 V, with no periphery protection on the device, demonstrating that localized epitaxy of GaN on Si has great potential for vertical high-power devices.**

## 1. Introduction

Power electronics have a wide range of applications, from devices operating at low voltages, for example, in portable electronics, to devices operating at high voltages, for example, in power transmission and distribution systems. Although during the past decades, devices based on silicon (Si) have dominated this field, wide-bandgap semiconductor materials, such as gallium nitride (GaN) and silicon carbide (SiC), have great potential to replace Si in electronic applications.[1] In particular, the 11 times higher breakdown electric field of GaN (GaN: 3.3 MV cm$^{-1}$, Si: 0.3 MV cm$^{-1}$) means that for a given film thickness, GaN-based devices can operate at voltages 11 times higher than their Si-based counterparts, and can be significantly smaller, giving potential for lower cost and higher frequency operation. In addition, the larger bandgap energy of GaN makes the devices capable to operate at temperatures greater than 300 °C, which are twice the maximum of those for Si-based components.[2]

Silicon carbide is an excellent alternative wide-bandgap semiconductor, however, GaN grown on 200 mm-diameter wafers remains an attractive option. The lower wafer and epitaxy cost, along with the lower technological barriers of processing large-diameter wafers, make Si wafers an excellent alternative to the native GaN substrates, which may show varying quality and limited availability.[3] Moreover, Si, when compared to other low-cost substrates, such as sapphire, shows good electrical and thermal conductivity. Nonetheless, it should be noted that the large lattice mismatch between GaN and Si causes structural defects and a high threading dislocation density in the grown GaN layer.[4]

For the growth of GaN on Si, buffer layers are necessary, first, because of the meltback etching effect between Ga and Si,[5] and second, to control the large tensile strain generated in the grown GaN layer, after cooling from the growth temperature, due to the large difference in the thermal expansion coefficients between GaN and Si. The buffer layers, AlN and AlGaN, introduce a compressive strain in the structure to compensate for this tensile strain.[6] For thicker GaN layers, it is difficult to maintain sufficient compressive strain in the layers, thus, limiting the thickness of crack-free GaN layers that can be achieved on planar

T. Kaltsounis, M. El Amrani, D. Plaza Arguello, H. El Rammouz, V. Maurya, M. Lafossas, S. Torrengo, H. Haas, L. Mendizabal, A. Gueugnot, D. Mariolle, T. Jalabert, J. Buckley, M. Charles
Université Grenoble Alpes
CEA, LETI
Grenoble 38000, France
E-mail: thomas.kaltsounis@cea.fr

T. Kaltsounis, Y. Cordier
Université Côte d'Azur
CNRS
CRHEA
Valbonne 06560, France

The ORCID identification number(s) for the author(s) of this article can be found under https://doi.org/10.1002/pssa.202400059.



**DOI: 10.1002/pssa.202400059**

Si wafers to 7 μm.[7] Localized epitaxial growth enables the relaxation of this tensile stress elastically, and thus, thicker GaN layers can be grown.

During localized epitaxial growth, Ga atoms diffuse on the mask toward the openings where growth takes place. As a result, the growth can expand both laterally, covering a part of the mask, and vertically with the formation of super elevations. That means that the thickness of the layers in the areas adjacent to the mask openings is greater than that at the center, thus, the thickness is not uniform. The extent of this phenomenon depends on the conditions and duration of the growth, but also on the mask area surrounding the openings. Another effect of this diffusion is the possible etching of the mask and the incorporation of atoms that are good n-type dopants of GaN, such as silicon and oxygen. Consequently, using conventional dielectrics such as $SiO_2$ or SiN for masking the growth leads to a final GaN layer with high unintentional doping.[8,9] In a previous study, we showed that using an $Al_2O_3$ mask, a very low unintentional doping concentration, around $10^{16}$ cm$^{-3}$, is achieved.[9]

Vertical power devices can be fabricated on these thicker GaN layers. To achieve greater breakdown voltages (BV) with the vertical configuration, it is sufficient to increase the thickness of the grown layers.[10] Furthermore, the thermal management of the vertical devices is easier, given that the electric field is more uniform and the current distribution is more spread.[11] Finally, the dynamic performance of such devices is improved, due to the fact that high carbon doping is not necessary to ensure insulating layers.

The operation at a voltage of 1200 V requires an n-doped GaN drift layer of thickness 10 μm with a low doping concentration in the order of $10^{16}$ cm$^{-3}$. This work is an intermediate step toward the achievement of these objectives. The purpose is to validate whether such a low doping concentration can be obtained after the selective area growth. In addition, the growth conditions of the layer are verified, by growing layers of half the target thickness, and ensuring that crack-free structures are grown. In this study, two samples are grown, one meant for the fabrication of a Schottky diode and one for a p-n diode, both as quasi-vertical devices. Capacitance–Voltage ($C$–$V$) measurements are used to extract the net doping concentration $N_D$-$N_A$ of the drift layer, and the breakdown voltage of the layer is measured by reverse bias $I$–$V$ measurements. Finally, scanning spreading resistance microscopy (SSRM) and scanning capacitance microscopy (SCM) are employed as techniques to electrically characterize the cross-section of the layer and provide spatial information on the doping concentration.

## 2. Experimental Section

The growth of the samples was carried out on a single-wafer AIXTRON Crius-R200 metal–organic vapor phase epitaxy tool, on 200 mm-diameter Si (111) wafers. Buffer layers of AlN and AlGaN, an undoped 300 nm-thick GaN layer, and three differently n-doped GaN layers were grown to serve as the template. The three GaN layers had a thickness of 350 nm each and their doping concentrations were $5 \times 10^{16}$, $5 \times 10^{17}$, and $5 \times 10^{18}$ cm$^{-3}$ from the bottom to the top of the template structure. The purpose of these layers is to serve as a reference for the evaluation of the doping concentration of the drift layer, during the measurements on the cross-section of the sample. A 50 nm-thick $Al_2O_3$ mask was deposited by atomic layer deposition at 300 °C on these layers, which was then patterned with photolithography and etched. Localized epitaxial growth was subsequently performed on the openings of this mask. Since their doping concentrations are known, the three n-doped GaN layers could be used as a reference for the characterization of the doping concentration of the regrown layer on the cross-section of the samples.

On both samples, an intentionally doped GaN layer was grown at 1040 °C, with a nominal growth rate of 1.5 μm h$^{-1}$ (for planar wafer growth). The pressure of the chamber was 400 mbar, the $NH_3$ flow was set at 10 slm and the growth time was 2 h. The dopant of the layer was Si and its intended doping concentration was $1 \times 10^{16}$ cm$^{-3}$. For the p-n diode, in addition, on top of the n-GaN layer, a 400 nm-thick p-type Mg-doped GaN layer was grown, with an intended concentration $4 \times 10^{18}$ cm$^{-3}$. The precursors for gallium, silicon, and magnesium were trimethyl gallium (TMGa), silane ($SiH_4$), and cyclopentadienyl-magnesium ($Cp_2Mg$), respectively. For Si doping, the $SiH_4$ flow rate value was set as that for a planar wafer growth. As the growth was selective, the $Al_2O_3$ mask was not removed after the growth. **Figure 1** shows a schematic of the sample grown for the fabrication of the quasi-vertical p-n diode.

Cross-sections were prepared by first cleaving the samples and then finalized by ionic polishing in a Leica TIC-3X tool.

SSRM is based on contact-mode atomic force microscopy (AFM) and it can provide an accurate spatial mapping of the doping concentration in a GaN layer. During the measurement, high forces may be applied on the tip to penetrate the oxide layer that can be formed on the surface, thus, doped-diamond-coated tips are used. The local resistivity of the sample can be extracted from the electrical current flowing through the biased surface and the conductive tip.[12] Since a current logarithmic amplifier with a range from 10 pA to 0.1 mA is used, the resistance of both high- and low-doped semiconducting regions can be measured.[13] The regrown GaN layer was contacted by applying silver paint to the bottom n-GaN layers, and the SSRM measurements were conducted in the air on a Bruker Dimension ICON AFM tool at atmospheric pressure.

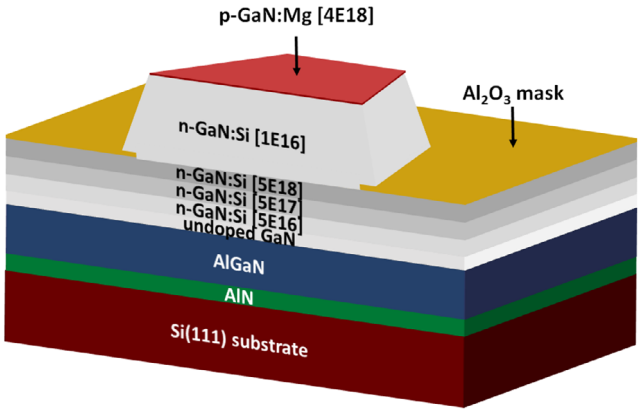


**Figure 1.** Schematic of the sample grown for the fabrication of the p-n diode.

SCM is also based on contact-mode AFM. Usually, this technique is used on an oxidized surface, to form a metal–oxide–semiconductor capacitor between the conductive tip, the oxide layer, and the semiconductor. However, the technique can be efficient in the absence of the oxide layer, like in this study, provided that a Schottky barrier is formed between the semiconductor and the tip.[14] An AC bias is applied to the tip, inducing capacitance changes in the doped layer, due to the accumulation or depletion of the carriers. A change in the local capacitance $\Delta C$ depends on the local carrier density, when there is a small change in the bias ($\Delta V$). The magnitude of this capacitance change may give information on the dopant concentration whereas the sign of the charges can be determined by the difference in phase between the capacitance change and the AC bias.[15]

Finally, anode and cathode contacts were deposited to fabricate the quasi-vertical devices. In the case of the p-n diode, the annealing of the p-layer by rapid thermal annealing was the first step. The Ni/Au (50/150 nm) metal stack was deposited as the anode contact and then annealed at 600 °C. Then, the $Al_2O_3$ mask around the mesa was etched by $Cl_2$, and Ti/Al/Ni/Au (95/200/20/265 nm) was deposited as the cathode contact. The cathode was not annealed to maintain a low thermal budget for the deposited anode contact. Despite the absence of annealing, the forward bias *I*–*V* measurements of the diodes demonstrated threshold voltages not limited by the behavior of the cathode contact which is expected to be ohmic. For the Schottky diode, the reversed process was followed, meaning that first, the $Al_2O_3$ mask was etched and the Ti/Al/Ni/Au cathode contact was deposited. Then it was annealed at 750 °C and, finally, the Ni/Au anode contact was deposited and annealed at 400 °C. Forward *I*–*V* measurements were used to examine the electrical behavior of the diodes, and reverse bias *I*–*V* measurements for the determination of the BV. In addition, the net doping concentration was extracted from the *C*–*V* measurements, using the $1\,C^{-2}$–V technique.

For the reference to the samples in the following sections, the name of the fabricated diode will be used. That means that the sample grown for the fabrication of a Schottky diode will be referred as the Schottky sample and the other as the p-n sample.

## 3. Results and Discussion

In this study, an existing mask was used for the localized growth of GaN. SSRM and SCM measurements were carried out on the cross-sections of 90 µm-diameter circular structures, which have different mask distances around them. **Figure** 2 shows the scanning electron microscopy (SEM) image of these structures on the p-n sample, and the patterns under study are noted on the image.

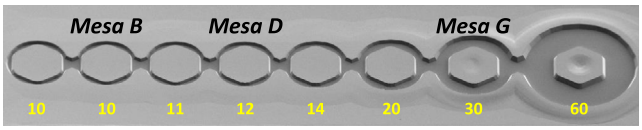


**Figure 2.** SEM image of the 90 µm-diameter circular structures with different mask distances around them on the p-n sample. The $Al_2O_3$ mask appears with the darker gray color and the mask distance in µm around each mesa is shown with the yellow color.

Due to lateral growth, the circular patterns change to a hexagonal shape, especially when the mask distance (the distance between both the central pattern area and the outside area where growth occurs) is increased. Moreover, it can be seen that the thickness across the diameter of the far-right structures is not uniform, and, in particular, as the mask distance increases, the thickness profile becomes less uniform. This is a result of the diffusion of the Ga atoms. As the mask area around the opening increases, more Ga atoms diffuse toward it, leading to the formation of super elevations at the edges of the patterns, which are obvious on the last two right mesas. Mesa B has a mask distance of 10 µm, mesa D and G have mask distances around them of 12 and 30 µm, respectively. These patterns were chosen to investigate if there would be an effect from the increasing size of the mask area around them on the doping concentration of the final structures.

First, the surface morphology of the two samples was investigated. **Figure 3**a shows the top-view AFM measurements on Mesa D on both samples. It can be seen that a crack-free surface is obtained after growth and the atomic steps can be observed. The root mean square surface roughness is 0.25 nm for the Schottky sample and 0.29 nm for the p-n sample.

Figure 3b shows the SSRM image obtained on the cross-section of the edge of Mesa D biased at −6 V. The bottom layers of known doping concentrations can be clearly distinguished and the progressive decrease of the resistance can be seen. The regrown GaN layer appears to have a uniform doping concentration, as intended. The change of color, and thus of the resistance, at the edge of the structure is probably an artifact from the measurement, rather than a significant change in the doping concentration itself. By comparing the resistances of the different layers, it is clear that the resistance of the regrown layer is higher than that of the layer of doping concentration $5 \times 10^{18}\,cm^{-3}$. Therefore, the doping concentration of the drift layer is definitely lower than $1 \times 10^{18}\,cm^{-3}$. However, it is challenging to determine the order of magnitude of the doping concentration of the regrown layer by referring to the lower n-GaN layers with doping concentrations of $5 \times 10^{17}$ and $5 \times 10^{16}\,cm^{-3}$. Further measurements are therefore required to determine the doping concentration of the regrown layer.

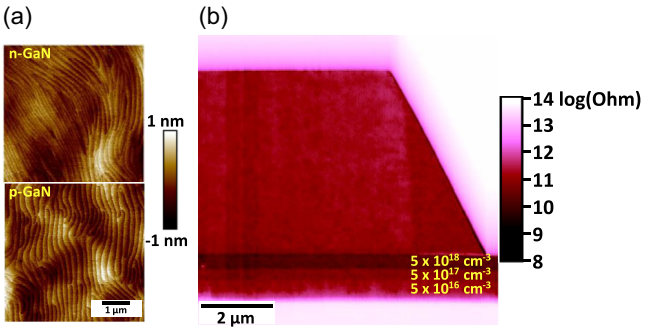


**Figure 3.** a) Top-view AFM measurements on Mesa D on the Schottky (top image) and on the p-n sample (bottom image) and b) SSRM measurement on the cross-section of the Schottky sample on the edge of mesa D biased at −6 V. The doping concentrations of the bottom layers are shown in yellow color.

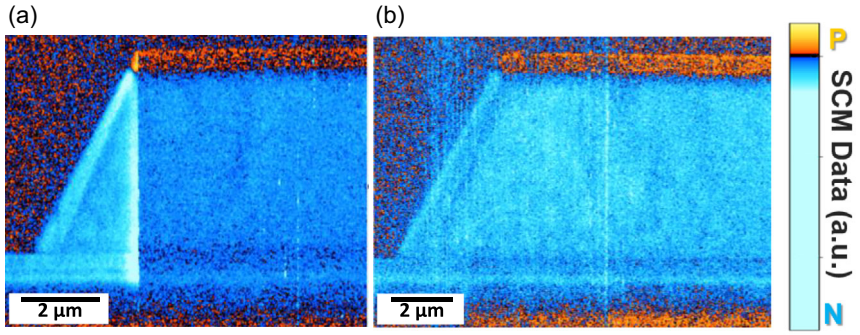


**Figure 4.** SCM measurements on the edge of the cross-section of a) Mesa B and b) Mesa G on the p-n sample under a DC bias of 0 V. P-doped regions are shown in orange, and, n-doped regions are shown in blue.

SCM was performed on the cross-section of the p-n sample, to evidence the n- and p-doped regions. **Figure 4** shows the SCM measurements on the edge of the cross-sections of Mesa B (a, left) and Mesa G (b, right). Both measurements were conducted under a DC bias of 0 V. The p-doped layer can be distinguished on the top of both structures as orange zones and the n-doped drift layer are illustrated by blue. It is worth mentioning that no p-doped region is observed at the edges of the structures and this result is currently not fully understood. Regarding the drift layer in Figure 4a, a change in the intensity of the signal at the edge of the structure is seen, but this is an artifact of the measurement, rather than a change in the doping concentration. In Figure 4b, a uniform signal is acquired for the n-doped drift layer.

For the fabrication of quasi-vertical devices, contacts were deposited on 90 and 140 µm-diameter circular structures. The mask distance around the structures was 10 µm. **Figure 5**a shows the optical microscopy image of the p-n diode fabricated on the 140 µm-diameter structure, which is within the dotted yellow circle. The anode contact is shown with the dark color and the circular cathode contact is illustrated by the bright yellow color. Stylus profilometry measurements were performed on the four structures to extract their thickness profiles. We can observe in Figure 5b that after the growth, the structures have a uniform thickness, of around 4.7 and 5.2 µm for the Schottky and p-n sample, respectively. From these measurements, we can deduce that the thickness of the p-doped layer is about 500 nm, which is higher than the nominal one by 100 nm, because of the extra material coming from the diffusion of the Ga atoms during the growth.

On these structures, forward and reverse *I*–*V* measurements were performed, to evaluate the electrical behavior of the diodes. The normalization of the current to extract the current density was with regard to the contact area. **Figure 6**a,b shows the forward *I*–*V* measurements on the four diodes in logarithmic and linear scale, respectively. Regarding the Schottky sample, at 6 V, the output current density for the 140 µm-diameter diode is 100 A cm$^{-2}$, whereas it is about 110 A cm$^{-2}$ for the 90 µm-diameter device. Regarding the p-n sample at the same voltage, the 90 µm-diameter diode delivered a current density of a little lower than 1 kA cm$^{-2}$, and the 140 µm-diameter diode achieved a current density of 120 A cm$^{-2}$. Moreover, as can be seen in Figure 6b, at 1 A cm$^{-2}$, the turn-on voltage for both the p-n diodes is about 3.3 V. For the Schottky diodes, the turn-on voltage is about 1 V.

Reverse *I*–*V* measurements were also performed to evaluate the destructive breakdown voltage of the quasi-vertical devices, as shown in Figure 6a. The compliance current, during the measurements, was set to 10 mA and the normalization for the calculation of the current density was with respect to the anode contact area. The BVs of the Schottky diodes were relatively low, 160 and 115 V for the 90 and 140 µm-diameter circular structures, respectively. In contrast, the p-n diodes showed much higher BVs. For the 90 µm-diameter structure, destructive BV occurred at 259 V,

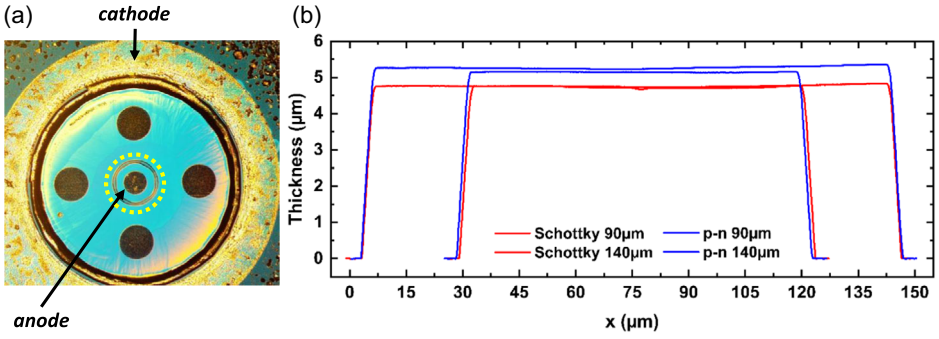


**Figure 5.** a) Optical microscopy image of the contacts deposited on the 140 µm-diameter structure on the p-n sample and b) stylus profilometry on 90 and 140 µm-diameter circular structures on the Schottky (red lines) and p-n (blue lines) samples.

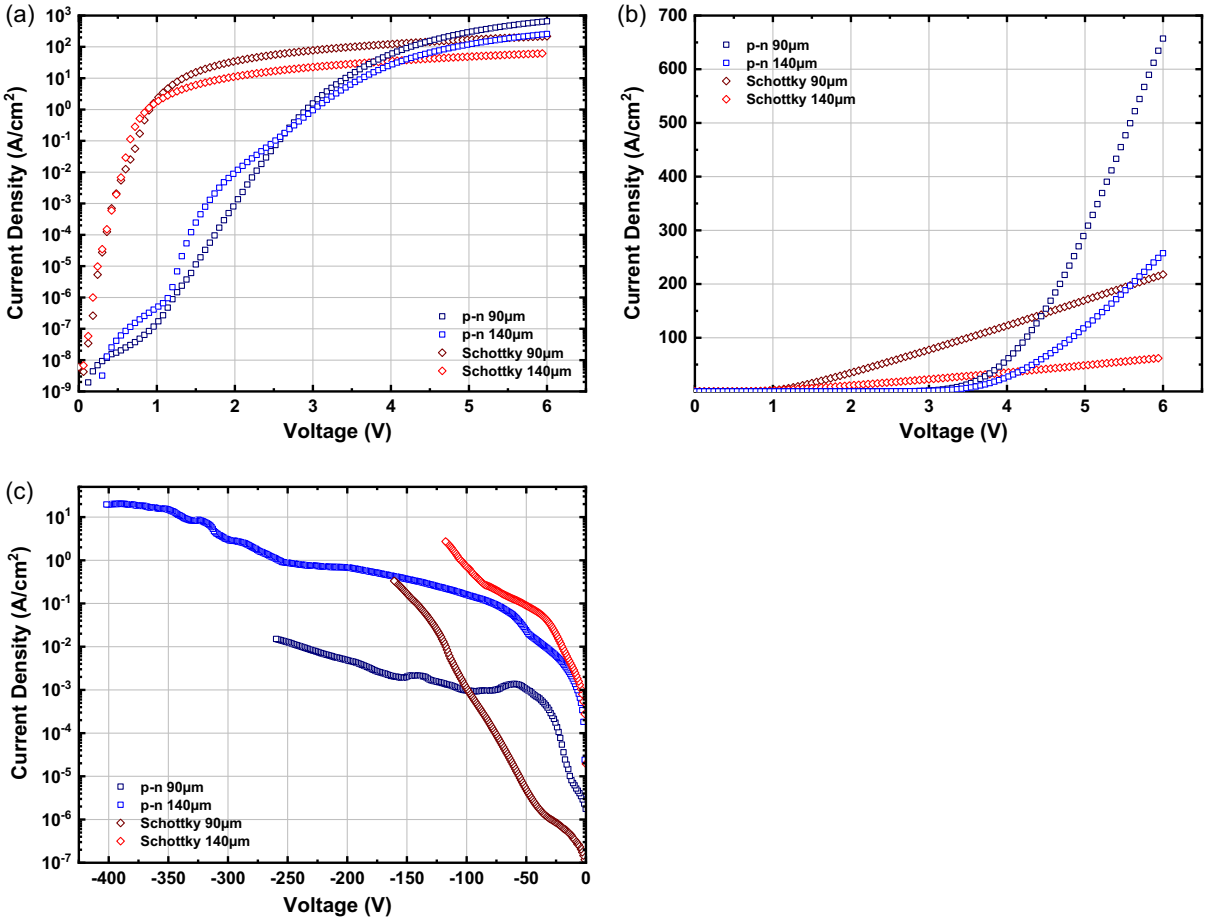


**Figure 6.** a) Forward in log scale, b) forward in linear scale, and c) Reverse *I–V* measurements of the 90 and 140 μm-diameter circular structures on the p-n and Schottky samples.

while for the 140 μm-diameter structure, the corresponding value was 402 V. This is a high BV value achieved for a p-n diode without any protection, and it is comparable to values reported in the literature for diodes fabricated on planar GaN layers grown on Si wafers. **Figure 7** shows the BV versus thickness of Schottky and p-n diodes fabricated on full wafer layers of GaN on Si wafers and of the p-n diode fabricated in this study.[16–32] The leakage current of the devices, in particular that of the 140 μm-diameter p-n diode, is quite high, however, it should be noted that no action was taken to limit it. Considering that no processing was performed for the periphery protection of the devices, this is a very promising result for the localized epitaxial growth of GaN-on-Si wafers.

Finally, *C–V* measurements were carried out on the two structures on the p-n sample to extract the net doping concentration of the drift layer. **Figure 8**a shows the $1\,C^{-2}$ plot against the voltage applied to the anode and the linear fitting for the extraction of the doping concentration. Figure 8b shows the net doping concentration versus the depletion width in the drift layer. The net doping concentration is found to be around $2.7 \times 10^{16}\,cm^{-3}$

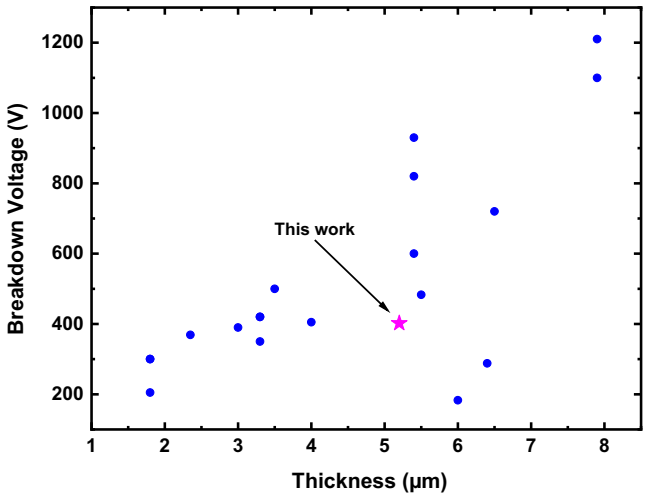


**Figure 7.** Breakdown voltage versus thickness of Schottky and p-n diodes fabricated on full wafer layers of GaN on Si wafers and of the p-n diode fabricated in this study.[16–32]

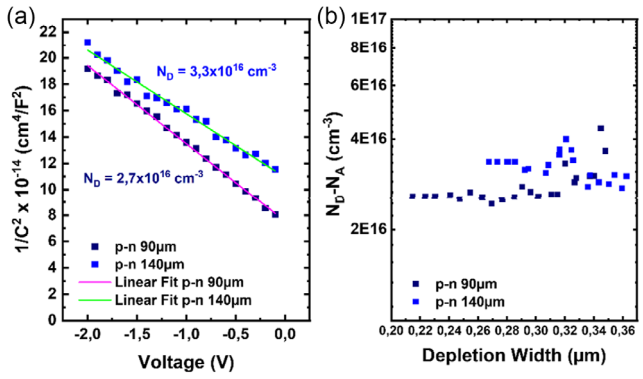


**Figure 8.** a) 1 $C^{-2}$ versus voltage and extracted net doping concentrations from the linear fitting and b) ($N_D$–$N_A$) versus depletion width for the 90 and 140 µm-diameter circular structures on the p-n sample.

and $3.3 \times 10^{16}\,cm^{-3}$ for the 90 µm-diameter and the 140 µm-diameter circular diode, respectively. A possible explanation of the present result is the contribution of donor impurities. Due to the absence of silicon in the mask, oxygen could be suspected to be the origin of the excess of donors. Also, at the present stage of the study, it is possible that the $SiH_4$ flow used for doping the drift layer is still too large and should be further reduced. Forthcoming studies will focus on these questions.

## 4. Conclusion

In this study, we grew two samples by localized epitaxy to fabricate quasi-vertical Schottky and p-n diodes. The SSRM showed a uniform doping concentration in the drift layer and the SCM measurements confirmed the successful localized epitaxy of n- and p-doped layers, in the case of the p-n sample. The net doping concentration of the drift layer was calculated from *C–V* measurements and it was found to be about $3 \times 10^{16}\,cm^{-3}$. This value is higher than that intended, and it may indicate that better adjustment of the $SiH_4$ flow is required for the growth of this layer. Through reverse *I–V* measurements, a breakdown voltage of 402 V was achieved for a quasi-vertical p-n diode fabricated on a 4.7 µm-thick drift layer, with no periphery protection. This value is the highest reported for a p-n diode grown by the localized epitaxial growth of GaN on Si wafers. It is validated that a low doping concentration can be obtained from the selective area growth of GaN layers on Si wafers, thus, a high breakdown voltage can be achieved. The next step would be the growth of GaN layers with doubled thickness since crack-free structures of half the targeted thickness were grown under the selected growth conditions. This is a very promising result toward the growth by localized epitaxy of GaN layers for the fabrication of high-power vertical devices operating at 1200 V.

## Acknowledgements

Part of this work, carried out on the Platform for Nanocharacterisation (PFNC), was supported by the "Recherches Technologiques de Base" program. This work is part of the **ELEGANT** project (ANR-22-CE05-0010).

## Conflict of Interest

The authors declare no conflict of interest.

## Data Availability Statement

The data that support the findings of this study are available from the corresponding author upon reasonable request.

## Keywords

GaN-on-Si, localized epitaxy, quasi-vertical diode, scanning capacitance microscopy, scanning spreading resistance microscopy

Received: January 15, 2024
Revised: April 9, 2024
Published online:

[1] F. Iacopi, M. Van Hove, M. Charles, K. Endo, *MRS Bull.* **2015**, *40*, 390.
[2] M. Meneghin, C. De Santi, I. Abid, M. Buffolo, M. Cioni, R. A. Khadar, L. Nela, N. Zagni, A. Chini, F. Medjoub, G. Meneghesso, G. Verzellesi, E. Zanoni, E. Matioli, *J. Appl. Phys.* **2021**, *130*, 18.
[3] L. Liu, J. H. Edgar, *Mater. Sci. Eng.* **2002**, *37*, 61.
[4] H. Amano, Y. Baines, E. Beam, M. Borga, T. Bouchet, P. R. Chalker, M. Charles, K. J. Chen, N. Chowdhury, R. Chu, C. De Santi, M. Merlyne De Souza, S. Decoutere, L. Di Cioccio, B. Eckardt, T. Egawa, P. Fay, J. J. Freedsman, L. Guido, O. Häberlen, G. Haynes, T. Heckel, D. Hemakumara, P. Houston, J. Hu, M. Hua, Q. Huang, A. Huang, S. Jiang, H. Kawai, et al. *J. Phys. D. Appl. Phys.* **2018**, *51*, 16.
[5] M. Khoury, O. Tottereau, G. Feuillet, P. Vennéguès, J. Zúñiga-Pérez, *J. Appl. Phys.* **2017**, *122*, 10.
[6] M. Charles, J. Kanyandekwe, S. Bos, Y. Baines, E. Morvan, A. Torres, F. Templier, M. Plissonnier, *ECS. Trans.* **2018**, *86*, 233.
[7] A. Tanaka, W. Choi, R. Chen, S. A. Dayeh, *Adv. Mater.* **2017**, *29*, 1.
[8] A. Debald, S. Kotzea, J. Riedel, M. Heuken, H. Kalisch, A. Vescan, *Phys. Status Solidi A* **2019**, *1900676*, 2.
[9] T. Kaltsounis, H. Haas, M. Lafossas, S. Torrengo, V. Maurya, J. Buckley, D. Mariolle, M. Veillerot, A. Gueugnot, L. Mendizaba, Y. Cordier, M. Charles, *Microelectron. Eng.* **2023**, *273*, 111964.
[10] J. Hu, Y. Zhang, M. Sun, D. Piedra, N. Chowdhury, T. Palacios, *Mater. Sci. Semicond. Process.* **2018**, *78*, 75.
[11] Y. Zhang, M. Sun, Z. Liu, D. Piedra, H. S. Lee, F. Gao, T. Fujishima, T. Palacios, *IEEE Trans. Electron Devices* **2013**, *60*, 2224.
[12] R. P. Lu, K. L. Kavanagh, St. J. Dixon-Warren, A. Kuhl, A. J. SpringThorpe, E. Griswold, G. Hillier, I. Calder, R. Arés, R. Streater, *J. Vac. Sci. Technol. B Microelectron. Nanom. Struct. Process. Meas. Phenom.* **2001**, *19*, 1662.
[13] R. A. Oliver, *Reports Prog. Phys.* **2008**, *71*, 17.
[14] C. Chen, S. Ghosh, F. Adams, M. J. Kappers, D. J. Wallis, R. A. Oliver, *Ultramicroscopy* **2023**, *254*, 113833.
[15] J. Sumner, R. A. Oliver, M. J. Kappers, C. J. Humphreys, *J. Appl. Phys.* **2009**, *106*, 10.
[16] Y. Zhang, M. Sun, D. Piedra, M. Azize, X. Zhang, T. Fujishima, T. Palacios, *IEEE Electron Device Lett.* **2014**, *35*, 618.
[17] Y. Zhang, D. Piedra, M. Sun, J. Hennig, A. Dadgar, L. Yu, T. Palacios, *IEEE Electron Device Lett.* **2017**, *38*, 248.
[18] X. Zhang, X. Zou, X. Lu, C. W. Tang, K. M. Lau, *IEEE Trans. Electron Devices* **2017**, *64*, 809.
[19] X. Zou, X. Zhang, X. Lu, C. W. Tang, K. M. Lau, *IEEE Electron Device Lett.* **2016**, *37*, 1158.

[20] Y. Zhang, M. Sun, H. Y. Wong, Y. Lin, P. Srivastava, C. Hatem, M. Azize, D. Piedra, L. Yu, T. Sumitomo, N. de Almeida Braga, R. Vidas Mickevicius, T. Palacios, *IEEE Trans. Electron Devices* **2015**, *62*, 2155.
[21] X. Liu, M. Wang, J. Wei, C. P. Wen, B. Xie, Y. Hao, X. Yang, B. Shen, *IEEE Trans. Electron Devices* **2023**, *70*, 1636.
[22] X. Guo, Y. Zhong, Y. Zhou, X. Chen, S. Yan, J. Liu, X. Sun, Q. Sun, H. Yang, *IEEE Electron Device Lett.* **2022**, *43*, 2057.
[23] F. Jia, X. Ma, L. Yang, X. Zhang, B. Hou, M. Zhang, M. Wu, X. Nui, J. Du, S. Liu, Y. Hao, *IEEE Electron Device Lett.* **2022**, *43*, 1400.
[24] Y. Li, M. Wang, R. Yin, J. Zhang, M. Tao, B. Xie, Y. Hao, X. Yang, C. P. Wen, B. Shen, *IEEE Electron Device Lett.* **2020**, *41*, 329.
[25] R. A. Khadar, C. Liu, L. Zhang, P. Xiang, K. Cheng, E. Matioli, *IEEE Electron Device Lett.* **2018**, *39*, 401.
[26] Y. Zhang, M. Yuan, N. Chowdhury, K. Cheng, T. Palacios, *IEEE Electron Device Lett.* **2018**, *39*, 715.
[27] X. Zhang, X. Zou, C. W. Tang, K. M. Lau, *Phys. Status Solidi Appl. Mater. Sci.* **2017**, *214*, 2.
[28] X. Zou, X. Zhang, X. Lu, C. W. Tang, K. M. Lau, *IEEE Electron Device Lett.* **2016**, *37*, 636.
[29] S. Mase, T. Hamada, J. J. Freedsman, T. Egawa, *IEEE Electron Device Lett.* **2017**, *38*, 1720.
[30] X. Guo, Y. Zhong, J. He, Y. Zhou, S. Su, X. Chen, J. Liu, H. Gao, X. Sun, Q. Zhou, Q. Sun, H. Yang, *IEEE Electron Device Lett.* **2021**, *42*, 473.
[31] A. Gan, X. Song, B. Sun, J. Zhang, S. Zhao, Z. Bian, *J. Phys. D: Appl. Phys.* **2022**, *55*, 265103.
[32] J. Chen, X. Song, Z. Liu, X. Duan, H. Wang, Z. Bian, J. Zhang, Y. Hao, *Appl. Phys. Express* **2021**, *14*, 11.